Conf-750335--51

THE DESIGN OF THE ZERO GRADIENT SYNCHROTRON BOOSTER II RING MAGNET

by

M. H. Foss, K. Thompson, R. J. Lari, and J. Simpson

For Presentation At:

Particle Accelerator Conference,
Washington, D. C., March 12-14, 1975

USERDA AUA USAEC

ARGONNE NATIONAL LABORATORY, ARGONNE, ILLINOIS

THE DESIGN OF THE ZERO GRADIENT SYNCHROTRON BOOSTER II RING MAGNET*

M. H. Foss, K. Thompson, R. J. Lari, J. Simpson
Argonne National Laboratory
Argonne, Illinois

Introduction

The booster program was undertaken at the Argonne National Laboratory Zero Gradient Synchrotron (ZGS) to increase the ZGS beam intensity. By using the transplanted Cornell University 2.2 GeV synchrotron as Booster I, it has been shown at the ZGS that more than one hundred turns of H^- ions can be injected and stripped to H^+ in a booster ring. In Booster II, this intense beam can be accelerated to 500 MeV. Several pulses from the booster, which can run at 60 Hz, will make one ZGS pulse. The Booster II ring magnet is now under construction.

The ring has six periods. Each period contains an FDF triplet and a D singlet. The dimensions, gradients and field strengths are given in Table I. The lattice parameters, to which the booster magnet must conform, are discussed in a separate paper.[1]

Table I

Magnet Parameters	Length (in)	$B_o^{-1} dB/dR$ (per in)
Straight section	54	
Defocusing magnet	26.151	-0.0812
Straight section	76	
Triplet		
Focusing magnet	34.458	0.0811
Defocus. magnet	54.724	-0.0812
Focusing magnet	36.510	0.0811
Radius of central orbit	145	
Gap		
height at cent. orbit	2.46	
useful width at inj.	4	
pole tip width	7.6	
Central magnetic field		
extraction	9.9 kG	
injection	2.8 kG	

Ideal Field

It is assumed that the desired midplane field is

$$B_x = 0; \quad B_y = B_o + B_1 R$$

where R is the radius from the center of curvature of the magnet, and B_1 the desired gradient. This field is produced by a scalar potential which can be written[2]

$$V = -B_o y + \frac{B_1}{4}\left[3y(R^2 + y^2)^{1/2} + (R^2 - 2y^2)\sinh^{-1} y/R\right]$$

The field given by the above equation differs from the field in an infinitely long straight magnet with the same midplane field by a few gauss in 10,000, 1 in. off of the midplane. Nevertheless, the field of a straight magnet is used for reference when field errors are dicussed.

*Work supported by U.S. Energy Res. and Dev. Admin.

Pole Tip Design

The field produced by a pole tip shape was calculated with the TRIM[3] magnet program. Initial runs with TRIM showed 1% effects due to the curvature of the magnet. It turned out that these effects were generated in the "edit" subroutine of the program, i.e., the calculation of the field from the vector potentials. A new edit was written, and it now appears that the effects of curvature are small. The results presented here were obtained using cylindrical geometry. The new "edit" includes the calculation of error fields, i.e., the difference between the calculated fields and those of an ideal straight magnet. This is the source for Figs. 1, 3, and 5.

Since the field must be good at injection, the pole tip shape was determined using infinite permeable steel. As a check on the high field performance, the "edit" also calculated the average flux density between any two mesh points on the steel surface. Saturation, in the steel with a packing factor of 0.95, was limited by keeping the average flux density, between mesh points on the steel surface, below 16,500 G when the the central field was 10,000 G.

The shape for the central region of the pole was calculated using the field required for the focusing magnets in the equations presented above. To simplify specification and construction, the outer regions of the pole tip surface are composed of tangent circles and straight lines. Shapes were inputted to TRIM as a set of connected straight lines which enclosed the same amount of steel as the desired curve shape. For manufacturing purposes, the pole surface consists of straight lines except for the circular arcs near the edges.

The pole tip shape was determined by cut and try using the 5,000 mesh point version of TRIM. To improve the resolution, all of the available mesh points were used to design each side of the pole independently. The error fields for the focusing magnet are shown in Fig. 1. The field errors for the central 2 in. have been set equal to zero and the results presented extend 0.7 in. from the midplane.

Magnet Steel Design

Focusing Magnets

A mesh was then constructed for the entire upper half of the focusing magnet. This is shown in Fig. 2. The results are summarized in Table II for infinite permeable and M-45 steel. The coil current is the same for all the rows in the table. This allows useful comparisons from one row to another, but of course the rows with infinite permeability must be scaled to the injection field of about 2,800 G. In the first row the higher order odd and even field errors are expressed in gauss per 10,000 G central field. These

errors are measured at the maximum orbit displacement which is 2 in. from the central orbit at injection.

The original plan was to construct the yoke with a uniform packing factor of 0.95. These results are given in row two of Table II. It was later decided to construct the magnets with the desired 145 in. radius by fanning the laminations. That is, the laminations are placed in contact at the inner radius of the yoke and the average space between laminations is allowed to increase with increasing radius. In the focusing magnets it proved worthwhile to increase the steel density near the outer radius of the pole. This was done by periodically inserting partial laminations from a radius of 147.2 in. to the outside radius of the yoke. The resulting construction was simplified compared to a uniform density core and reduces the interlamination flux. The third row of Table II gives the results for the fanned yoke. Fig. 5 shows the field errors for this yoke and the corresponding flux map is shown in Fig. 4.

Defocusing Magnets

For simplicity and economy, the same pole tip shape was used for the defocusing magnets as was used for the focusing magnets. The curvature of the magnets introduces small differences in the central field, in the magnitude of the gradient, and in the errors, as compared to the focusing magnets. This may be seen by comparing the first and fourth rows of Table II. The high field results for the uniform (0.95 packing factor) yoke and the fanned yoke are given in rows 5 and 6 of Table II. The fanned construction was used here also, but no partial laminations were inserted on the high field side. The high field errors are shown in Fig. 5, and the corresponding flux map is shown in Fig. 6. It is interesting to note, in Figs. 1, 3, and 5, that the edge errors present with infinite permeability can also be seen at high field, of course, on the opposite side in the defocusing magnet.

Magnet Coil Design

A preliminary coil configuration was developed concurrent with the magnet steel design. A final coil was then designed to provide the required 34270 At rms. The conductor used was 0.289 in.^{2} x 0.161 in. ID oxygen-free solid copper. It was originally required that an existing motor generator, 30 Hz power supply rated at 3000 V maximum, and an existing 5000 A dc power supply be used to drive the 12 magnets of the booster ring connected in series. These power supply limits necessitated that the coil in each magnet effectively has only seven turns.

An interactive computer program[4] was used to establish the conductor operating parameters for a triplet magnet. Considerations of water pressure and temperature gradient limitations resulted in each conductor carrying no more than 272 A rms. To provide the ampere turns required, a total of 18 seven-turn circuits was used which were electrically and hydraulically connected together in parallel. Only two nonconducting hoses were used in this design and a single conductor connected adjacent magnets.

The field calculations assumed equal currents in all conductors in the coil. Since the currents vary during operation, the resistances of the parallel paths and also the inductances must be closely matched. The flux plot in Fig. 6 shows that turns located in various parts of the coil link different amounts of flux. By connecting turns with low flux linkage to turns with high values it was possible to provide 18 circuits which differed by only a few tenths of a percent. The results of the final TRIM calculations described above for both core geometries were used to estimate the flux linked by each turn. The calculated vector potentials at the mesh points inside the coil were interpolated at the center of each conductor. These vector potentials were then converted to the flux linked by each turn. These results were summed in various groups of seven turns and the differences noted.

See Fig. 7 for the final arrangement of the 126 turns of conductor in each magnet. Each of the twelve layers contains three separate conductors. Four different symbols are used to identify four of the seven-turn circuits. It can be seen in this figure how the turns close to the midplane are connected to turns far from the midplane, and how turns close to the pole are connected to turns far from the pole. The most uniform flux linkages for the 18 circuits were obtained with the layers marked A in Fig. 7 shifted towards the pole. This resulted in 4% differences in the dc resistances of the circuits in a singlet magnet. The final coil geometry shown results in circuits having maximum differences of about 0.7% in both the dc resistances and in the flux linkages. This geometry also facilitates the coil winding and the interconnections.

The differences in flux linkages give rise to differences in the impedances for the parallel connected circuits in each magnet. As a result there are different currents in various parts of the seven-turn coil. This current is an eddy current in the coil. Estimates of these eddy currents are 1.4 A and 0.8 A for each conductor in a singlet and a triplet magnet. Estimates were also made of the eddy currents generated within the conductors. This resulted in a power loss of about 7 kW for the Booster II ring, excluding the coil ends.

After the ring magnet design was completed, a decision was made to custom build a power supply for the Booster II ring. As a result, an increase in the magnet inductances by a factor of four was required. This greatly reduces the cost of the power supply, power distribution network, resonating capacitors, and low pass filter. This increase in inductance was easily accomplished by increasing the number of effective turns for the magnets to 14. Fig. 8 shows the final electrical and hydraulic connections of the magnets. The final coil design contains two segments of nine parallel-connected, seven-turn conductors. These two are then connected in series.

Acknowledgments

The authors wish to thank W. F. Praeg for his many helpful discussions and A. J. Lisack for his help in visualizing the many coil designs.

References

1. E. A. Crosbie, M. H. Foss, T. K. Khoe, J. Simpson, Argonne National Laboratory, The Design of the Zero Gradient Synchrotron Booster II Lattice, see this conference proceedings.

2. Martyn H. Foss, Mathematical Techniques for Designing Field Shapes, Carnegie Institute of Technology (July 11, 1951), report number NYO 911.

3. Alan M. Winslow, Magnetic Field Calculations in an Irregular Triangle Mesh, First International Conference on Magnet Technology, SLAC (September 1965), p 170.
   John S. Colonias, Joseph H. Dorst, Magnet Design Applications of the Magnetostatic Program Called TRIM, ibid., p 188.

4. Kenneth M. Thompson, An Interactive Code for Optimization of the Design of Water-Cooled Conductors, Fourth International Conference on Magnet Technology, BNL (September 1972), p 725.

Table II

Field Errors

Magnet Type	Yoke	Field (G)	Quadrupole $B^{-1}\, dB/dR$ (in^{-1})	Sextupole $B^{-1}\, d^2B/dR^2$ (in^{-2})	Maximum Orbit Displacement, Δx (in)	Odd Higher Order Field Error at Δx (G)	Even Higher Order Field Error at Δx (G)
F	μ = 00	10,000	0.08111	-0.00012	2.0	-3.5	-2.5
F	uniform steel	9,845	0.08089	-0.00029	0.9	-0.1	+0.1
F	fanned steel	9,705	0.08073	-0.00049	0.9	-0.1	+0.2
D	μ = 00	9,997	-0.08120	-0.00020	1.7	+0.7	-1.1
D	uniform steel	9,841	-0.08117	-0.00024	0.8	-0.0	-0.0
D	fanned steel	9,713	-0.08108	-0.00036	0.8	+0.3	-0.1

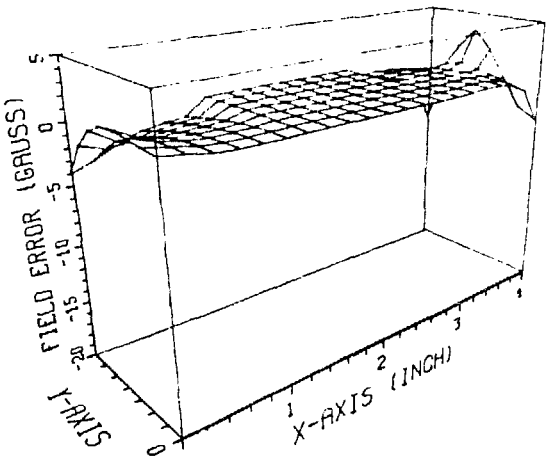

Fig. 1 Focusing magnet field errors for [illegible] the central field is 10000 G at x = 2.

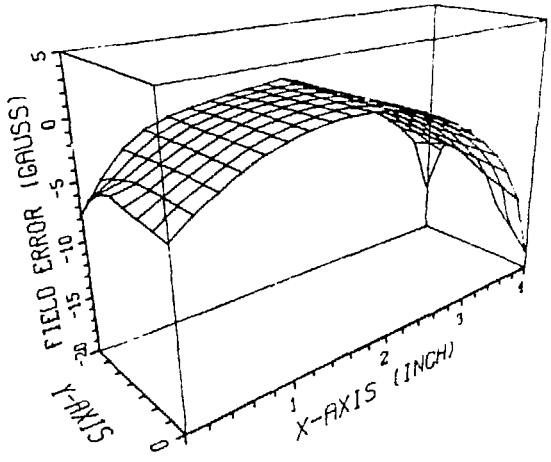

Fig. 3 Focusing magnet field errors for finite permeable steel with fanned yoke. The central field is 9705 G at x = 2.

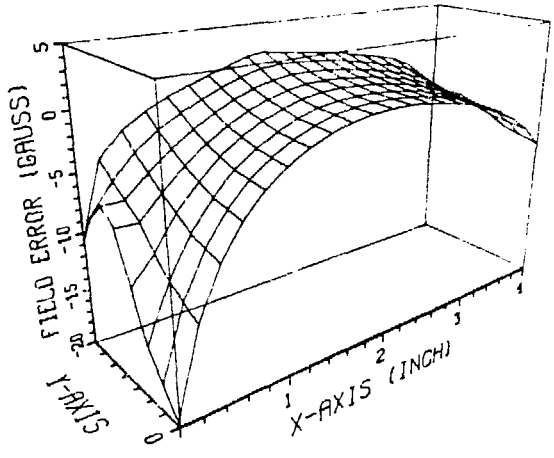

Fig. 5 Defocusing magnet field errors for finite permeable steel with fanned yoke. The central field is 9713 G at x = 2.

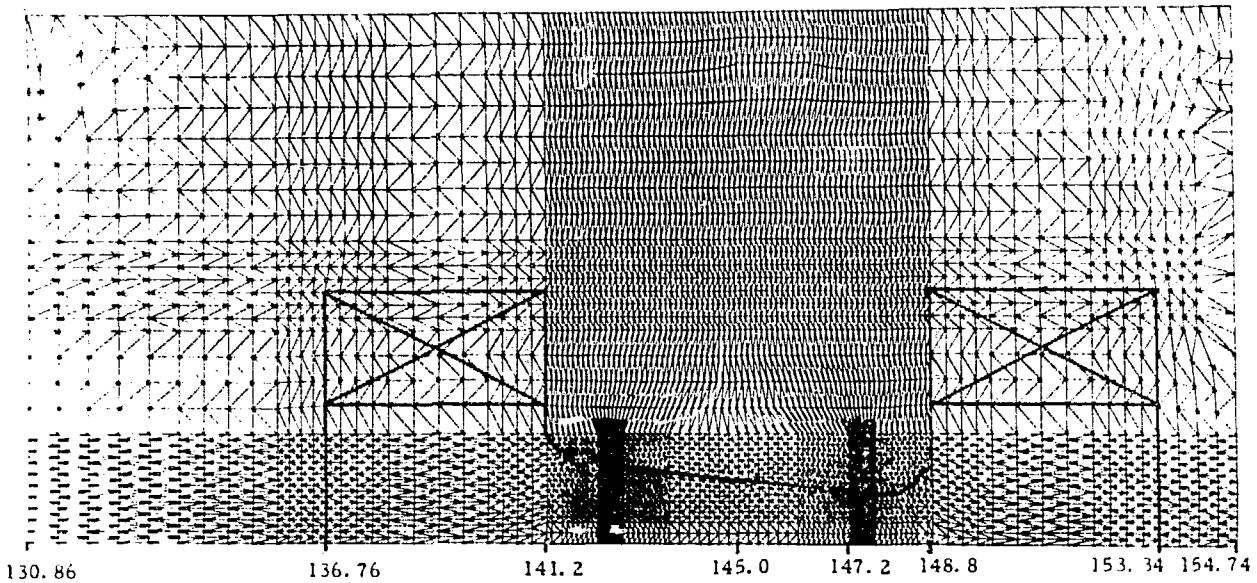

Fig. 2 Mesh used by TRIM for the focusing magnet

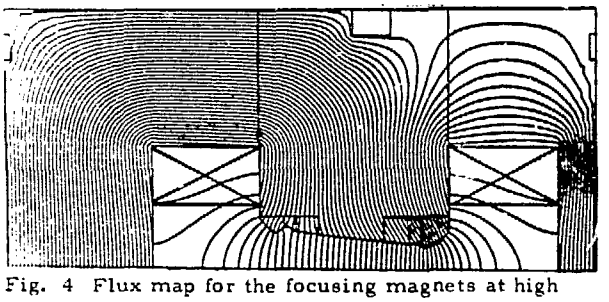

Fig. 4 Flux map for the focusing magnets at high field.

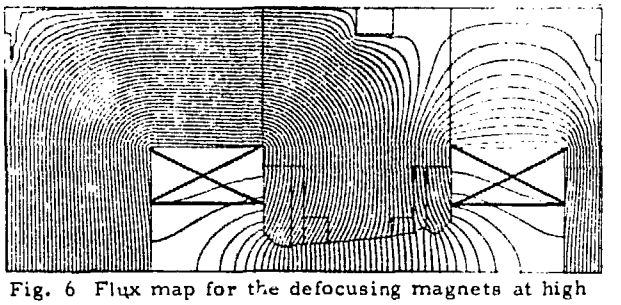

Fig. 6 Flux map for the defocusing magnets at high field.

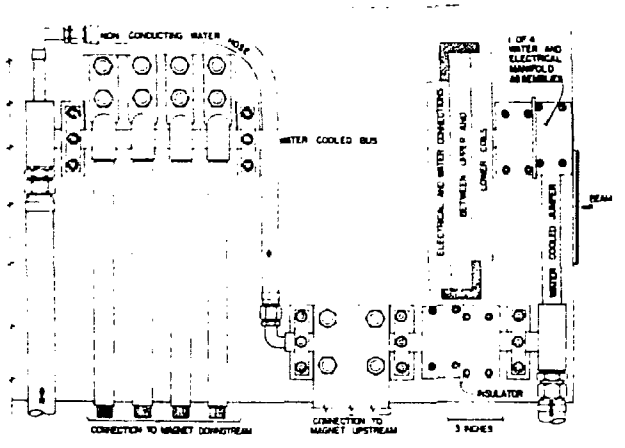

Fig. 7 View of inside radius area of the main ring magnets showing all electrical and water connections.

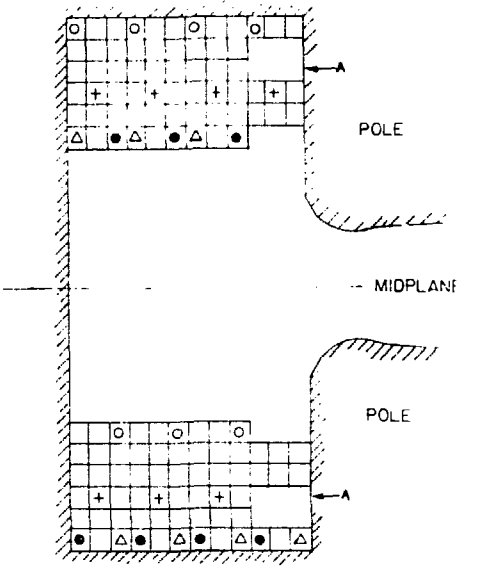

Fig. 8 Schematic of coil geometry with the locations shown for the conductors in four, seven turn, circuits.